# A study of two onramp metering schemes for congested freeways [1]

Gabriel Gomes[2] and Roberto Horowitz[3]
Department of Mechanical Engineering
University of California at Berkeley
Berkeley, CA 94720-1740

**Abstract**

We investigate the stability of a nonlinear (piecewise linear and possibly discontinuous) model of a freeway onramp, controlled by two popular onramp metering schemes: Alinea and Percent-Occupancy. The freeway model is based on Daganzo's cell-transmission model and can be understood as a hybrid system switching among several discrete-time linear dynamic equations. It is shown, under conditions placed on the upstream mainline demand and on the controller parameters, that both of these controllers are capable of rejecting congestion near the onramp. In addition, we illustrate how the use of downstream measurements allows Alinea to robustly drive the freeway to a predetermined uncongested desired state.

## 1 Introduction

The purpose of this article is to construct a suitable model for the analysis of local, traffic-responsive ramp metering controllers, and to use it to gain insight into the behavior of two such control schemes, namely, Alinea and Percent-Occupancy (%-Occ). The onramp configuration considered here is shown in Fig. 1. Vehicles access the freeway from a right-side onramp. They join the mainline flow by changing lanes within the merge section. This influence is represented in the figure by a distribution of vertical arrows. Congestion appears whenever the demands on the freeway section (mainline and onramp) exceed its capacity. The point at which congestion begins is termed the *bottleneck*. It is typically somewhere within the merge section or nearby downstream. From this point, congestion propagates upstream, while the portion of the freeway downstream of the bottleneck remains uncongested.

Several authors have reported on an apparent "two-capacity phenomenon" [1, 2], in which the flow out of a bottleneck during congestion (also known as the *queue discharge rate*) is less than the maximum observed flow during freeflow. This observation was identified in [3] as a primary motivation for regulating the onramp flow, since it provides an incentive for keeping the mainline uncongested. A reasonable requirement for models used to analyze onramp controllers is therefore that they capture this observed attribute of freeway traffic behavior.

The geometric features represented in Fig. 1 suggest a division of the freeway into three zones: `A`, `B` and `C`, separated respectively by the bottleneck and the onramp junction. One of the issues considered in this paper is the placement of the mainline sensor. Placing it in zone `A` is an obviously bad choice, since the flow out of the bottleneck becomes a constant whenever zone `B` becomes congested. Thus, the density of the freeway upstream of the bottleneck is *unobservable* from zone `A` during congestion. If the sensor is placed in zone `B`, it gains observability in the congested regime. However, as it is moved upstream through zone `B`, a delay appears between the onset of congestion and its effect on the measurements. With the sensor placed in zone `C`, the mentioned delay is large and the density in zones `B` and `A` are unobservable during freeflow.

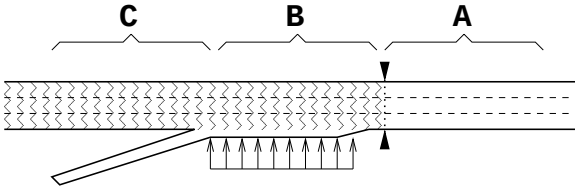


**Figure 1:** Detector placement zones

The model used here is an application of the principles of the cell-transmission model presented in [4, 5]. The variation that has been introduced allows it to more easily capture the two-capacity phenomenon (discontinuity) which is considered essential to the analysis of onramp metering control algorithms. By chosing sections to coincide with the zones of Fig. 1, the model is also capable of reproducing the two other important features mentioned above: the influence of detector location on observability, and the delayed backward propagation of congestion. Two significant limitations of the presented model are 1) it does not consider the

[1]Research supported by UCB-ITS PATH grant TO4136
[2]Graduate student, gomes@me.berkeley.edu
[3]Professor, horowitz@me.berkeley.edu; corresponding author

saturation limits typically applied to onramp metering rates, and 2) it does not keep track of the length of the onramp queue, and therefore cannot incorporate queue length constraints.

## 2 Freeway modeling

We use the principles of the well-known cell-transmission model [4, 5] to construct a mathematical description of the single onramp configuration of Fig. 2. The freeway mainline in the vicinity of the onramp is partitioned into four sections (0 through 3), or *cells* in the terminology of [4], with the onramp connected to the mainline at section 1.

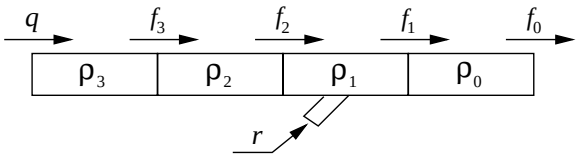


**Figure 2:** Single onramp configuration

Sections 0, 1, and 2 coincide with zones `A`, `B`, and `C` in the Fig. 1. The state of the freeway is composed of section densities $\rho_{i[k]}$ ($k$ is a time index), in vehicles per section. These states are governed by the principle of conservation of vehicles. The term *congestion* is defined as the condition of a section $i$ whose density exceeds a critical value $\rho_c$, which is assumed uniform along the freeway. An important assumption made here is that the boundary sections (0 and 3) remain *uncongested* at all times (i.e. $\rho_{i[k]} < \rho_c$ for $i = 0, 3$). This amounts to a restriction on the magnitude of the upstream flow $q_{[k]}$ and on the state of the freeway downstream of section 0, and is required in order to establish consistent boundary conditions for the system. It is also assumed that $q_{[k]}$ remains constant, or at least converges to a constant $q$ over time.

Inter-cellular flows ($f_{i[k]}$ in vehicles per time interval) are given by:

$$f_{i[k]} = \begin{cases} v\rho_{i[k]} & \text{if } \begin{cases} i \text{ Uncongested} \\ i{-}1 \text{ Uncongested} \end{cases} \\ \texttt{min}(v\rho_{i[k]}, \\ w(\rho_j - \rho_{i-1[k]}) - \alpha_i r_{[k]}) & \text{if } \begin{cases} i \text{ Uncongested} \\ i{-}1 \text{ Congested} \end{cases} \\ f_d & \text{if } \begin{cases} i \text{ Congested} \\ i{-}1 \text{ Uncongested} \end{cases} \\ w(\rho_j - \rho_{i-1[k]}) - \alpha_i r_{[k]} & \text{if } \begin{cases} i \text{ Congested} \\ i{-}1 \text{ Congested} \end{cases} \end{cases}$$

This function $f_i(\rho_{i[k]}, \rho_{i-1[k]})$ differs from its counterpart in the cell-transmission model only in the ($i$ Uncongested) & ($i{-}1$ Congested) regime, where it equals $f_d$, the *queue discharge rate*. Thus, in contrast to the cell-transmission model, $f_i(\rho_{i[k]}, \rho_{i-1[k]})$ is allowed to be discontinuous, for example, if $f_d$ is chosen less than $v\rho_c$. The minimization rule of the cell-transmission model (Eq. 1b in [4]), on the other hand, ensures continuity of the flow function. This modification was introduced in order to incorporate the "jump discontinuity" observed in flow/density curves for freeways approaching capacity flow levels [1, 2].

Parameters $v$ and $w$ are, respectively, the normalized freeflow and congestion wave speeds. Both are in $(0, 1]$. $\alpha_i$ is a parameter that determines the direct influence of onramp flows on inter-cellular flows. For cells without onramps ($i = 0, 2, 3$), $\alpha_i$ is naturally set to zero. $\alpha_1$ is restricted to the range $[0, 1]$, and is henceforth denoted simply as $\alpha$. The parameters of the model are assumed to be related by Eq. (1), which stems from the interpretation illustrated in Fig. 3.

$$v\rho_c = w(\rho_j - \rho_c) > f_d \tag{1}$$

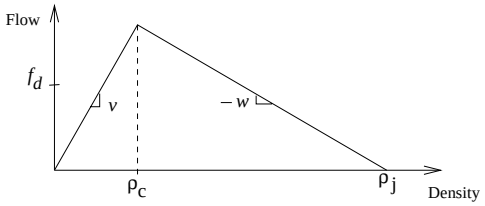


**Figure 3:** Interpretation of model parameters

Given the uncongested state in sections 0 and 3, the system as a whole can at any time be in one of four *congestion modes*: `UU`, `UC`, `CU` and `CC`, where the first letter indicates the state (`U`ncongested or `C`ongested) of section 2, and the second of section 1. In these modes, and following the definition of $f_{i[k]}$ given above, the inter-cellular flows take on values shown in Table 1.

**Table 1:** Four congestion modes

| | $f_{3[k]} =$ | $f_{2[k]} =$ | $f_{1[k]} =$ |
|---|---|---|---|
| `UU` | $v\rho_{3[k]}$ | $v\rho_{2[k]}$ | $v\rho_{1[k]}$ |
| `CU` | `min` $\{v\rho_{3[k]}$ , $w(\rho_j - \rho_{2[k]})\}$ | $f_d$ | $v\rho_{1[k]}$ |
| `UC` | $v\rho_{3[k]}$ | `min` $\{v\rho_{2[k]}$ , $w(\rho_j - \rho_{1[k]}) - \alpha r_{[k]}\}$ | $f_d$ |
| `CC` | `min`$\{v\rho_{3[k]}$ , $w(\rho_j - \rho_{2[k]})\}$ | $w(\rho_j - \rho_{1[k]}) - \alpha r_{[k]}$ | $f_d$ |

A total of six different combinations of expressions for flows $f_{1[k]}$, $f_{2[k]}$, and $f_{3[k]}$ can occur. These *dynamic modes* are denoted `I` through `VI`. They are given, along with their associated congestion modes in Table 2.

The remaining component of the dynamic model is the principle of vehicle conservation for each of the four sections. Because section 0 is assumed to remain in an uncongested state, it will not play a part in the stability analysis, and is therefore not considered further. The


Proceedings of the American Control Conference
Denver, Colorado June 4-6, 2003

**Table 2:** Six dynamic modes

| | $f_{3[k]} =$ | $f_{2[k]} =$ | $f_{1[k]} =$ |
|---|---|---|---|
| UU-I | $v\rho_{3[k]}$ | $v\rho_{2[k]}$ | $v\rho_{1[k]}$ |
| CU-II | $v\rho_{3[k]}$ | $f_d$ | $v\rho_{1[k]}$ |
| CU-III | $w(\rho_j - \rho_{2[k]})$ | $f_d$ | $v\rho_{1[k]}$ |
| UC-IV | $v\rho_{3[k]}$ | $v\rho_{2[k]}$ | $f_d$ |
| UC/CC-V | $v\rho_{3[k]}$ | $w(\rho_j - \rho_{1[k]}) - \alpha r_{[k]}$ | $f_d$ |
| CC-VI | $w(\rho_j - \rho_{2[k]})$ | $w(\rho_j - \rho_{1[k]}) - \alpha r_{[k]}$ | $f_d$ |

conservation equations are:

$$\begin{aligned}\rho_{1[k+1]} &= \rho_{1[k]} + f_{2[k]} - f_{1[k]} + r_{[k]} \\ \rho_{2[k+1]} &= \rho_{2[k]} + f_{3[k]} - f_{2[k]} \\ \rho_{3[k+1]} &= \rho_{3[k]} + q_{[k]} - f_{3[k]}\end{aligned} \tag{2}$$

Equation (2) and Table 2 constitute a complete model for the freeway/onramp system. The model switches among 7 finite states (UU-I, CU-II, CU-III, UC-IV, UC-V, CC-V, and CC-VI), and evolves within each one according to a discrete-time linear dynamics. Each of these dynamic modes are cast in a state-space form,

$$\rho_{[k+1]} = A^x \rho_{[k]} + B^x r_{[k]} + W^x \tag{3}$$

with $\rho_{[k]} = [\rho_{1[k]}, \rho_{2[k]}, \rho_{3[k]}]^T$, $x = \mathtt{I} \ldots \mathtt{VI}$, and matrices $A^x$, $B^x$, and $W^x$ given in Table 3.

**Table 3:** State-space representations

| $x$ | $A^x$ | $B^x$ | $W^x$ |
|---|---|---|---|
| I | $\begin{bmatrix} 1-v & v & 0 \\ 0 & 1-v & v \\ 0 & 0 & 1-v \end{bmatrix}$ | $\begin{bmatrix} 1 \\ 0 \\ 0 \end{bmatrix}$ | $\begin{bmatrix} 0 \\ 0 \\ q \end{bmatrix}$ |
| II | $\begin{bmatrix} 1-v & 0 & 0 \\ 0 & 1 & v \\ 0 & 0 & 1-v \end{bmatrix}$ | $\begin{bmatrix} 1 \\ 0 \\ 0 \end{bmatrix}$ | $\begin{bmatrix} f_d \\ -f_d \\ q \end{bmatrix}$ |
| III | $\begin{bmatrix} 1-v & 0 & 0 \\ 0 & 1-w & 0 \\ 0 & w & 1 \end{bmatrix}$ | $\begin{bmatrix} 1 \\ 0 \\ 0 \end{bmatrix}$ | $\begin{bmatrix} f_d \\ w\rho_j - f_d \\ q - w\rho_j \end{bmatrix}$ |
| IV | $\begin{bmatrix} 1 & v & 0 \\ 0 & 1-v & v \\ 0 & 0 & 1-v \end{bmatrix}$ | $\begin{bmatrix} 1 \\ 0 \\ 0 \end{bmatrix}$ | $\begin{bmatrix} -f_d \\ 0 \\ q \end{bmatrix}$ |
| V | $\begin{bmatrix} 1-w & 0 & 0 \\ w & 1 & v \\ 0 & 0 & 1-v \end{bmatrix}$ | $\begin{bmatrix} 1-\alpha \\ \alpha \\ 0 \end{bmatrix}$ | $\begin{bmatrix} w\rho_j - f_d \\ -w\rho_j \\ q \end{bmatrix}$ |
| VI | $\begin{bmatrix} 1-w & 0 & 0 \\ w & 1-w & 0 \\ 0 & w & 1 \end{bmatrix}$ | $\begin{bmatrix} 1-\alpha \\ \alpha \\ 0 \end{bmatrix}$ | $\begin{bmatrix} w\rho_j - f_d \\ 0 \\ q - w\rho_j \end{bmatrix}$ |

### 2.1 Controlability and Observability

The observability and controlability properties of the model outlined above will determine the ability of any onramp metering scheme to effectively influence traffic conditions on the freeway. Here we investigate how the model parameters ($v$, $w$, and $\alpha$) and the position of the feedback detector affect these properties. It is assumed that the mainline sensor is located either in zone B or in zone C (Fig. 1), by considering as output of the model either $\rho_1$ or $\rho_2$. Under each of these assumptions, the observability of each of the 6 dynamic modes is dictated by observability matrices $O_1^x$ and $O_2^x$ ($x$=I ... VI),

$$O_1^x = \begin{bmatrix} C_1 \\ C_1 A^x \\ C_1 (A^x)^2 \end{bmatrix} \qquad O_2^x = \begin{bmatrix} C_2 \\ C_2 A^x \\ C_2 (A^x)^2 \end{bmatrix}$$

with $C_1 = [1, 0, 0]$ and $C_2 = [0, 1, 0]$. Similarly, controlability is determined by the range of controlability matrices $P^x = [B^x, A^x B^x, (A^x)^2 B^x]$. The state variables that can be controlled and uniquely reconstructed in each dynamic mode are given in Table 4.

**Table 4:** Controlable and uniquely recontructable state variables in each dynamic mode ($\{\rho\}$ denotes $\{\rho_1,\rho_2,\rho_3\}$)

| | Controlable | Reconstructable from $\rho_2$ | Reconstructable from $\rho_1$ |
|---|---|---|---|
| I | $\{\rho_1\}$ | $\{\rho_2,\rho_3\}$ | $\{\rho\}$ |
| II | $\{\rho_1\}$ | $\{\rho_2,\rho_3\}$ | $\{\rho_1\}$ |
| III | $\{\rho_1\}$ | $\{\rho_2\}$ | $\{\rho_1\}$ |
| IV | $\{\rho_1\}$ | $\{\rho_2,\rho_3\}$ | $\{\rho\}$ |
| V | $\{\rho_1,\rho_2\}$ $\alpha \neq 1$<br>$\{\rho_2\}$ $\alpha = 1$ | $\{\rho\}$ $w \neq v$<br>$\{\rho_2,\rho_1+\rho_3\}$ $w = v$ | $\{\rho_1\}$ |
| VI | $\{\rho\}$ $\alpha \neq 1$<br>$\{\rho_2,\rho_3\}$ $\alpha = 1$ | $\{\rho_1,\rho_2\}$ | $\{\rho_1\}$ |

Notice in Table 4 that $\rho_1$ cannot be uniquely determined from $\rho_2$ whenever section 1 is uncongested (i.e. in modes I, II, and III). This is also the case in mode IV and in a degenerate case of mode V. Also notice that the choice of $\alpha$ affects the controllability of the model in congested modes V and VI. Specifically, $\alpha = 1$ results in a loss of controlability of $\rho_1$ during congestion.

## 3 Onramp control strategies

The control objective considered in this study is twofold. First, the controller should dissipate congestion by driving the freeway state from any initial state to UU-I. Second, once in UU-I, the controller should stabilize the linear system about a target state such that $v\rho_{1ss} > f_d$. That is, the steady-state throughput should exceed the queue discharge rate, which is assumed to be the throughput if no control is applied.

We investigate how well, and under what conditions on the controller parameters, the %-Occ and Alinea control laws accomplish these tasks.

### 3.1 %-Occ control

%-Occ control is a popular approach in the U.S. due to its simplicity of implementation and observed effectiveness. Similarly to Alinea, it falls under the category of local, traffic-responsive controllers, since it only

uses measurements in the direct vicinity of the onramp under control. It is distinguished from Alinea by the fact that, in most applications, the feedback sensor is placed upstream of the onramp junction. %-Occ can be interpreted as proportional feedback of the *occupancy* measurement. Occupancy is defined as the portion of time during which a loop detector registers a vehicle presence. It is closely related to the density states of the model described here. The control law for %-Occ can be written as:

$$r_{[k]} = K_1 - K_2 \rho_{2[k]} \tag{4}$$

where $K_1$ and $K_2$ are tunable controller parameters. The closed-loop dynamics under %-Occ (i.e. proportional) control is given by:

$$\rho_{[k+1]} = A^x_{occ}\rho_{[k]} + B^x_{occ} \tag{5}$$

with $A^x_{occ} = A^x - K_2 B^x C_2$ and $B^x_{occ} = W^x + K_1 B^x$ ($x = \texttt{I} \ldots \texttt{VI}$). We derive conditions on the model and controller parameters under which the %-Occ strategy accomplishes the stated objectives. To illustrate the methodology, consider mode `UC-V`, with closed-loop dynamics:

$$\rho_{[k+1]} = \begin{bmatrix} 1-w & -(1-\alpha)K_2 & 0 \\ w & 1-\alpha K_2 & v \\ 0 & 0 & 1-v \end{bmatrix} \rho_{[k]} + \begin{bmatrix} (1-\alpha)K_2 + w\rho_j - f_d \\ \alpha K_1 - w\rho_j \\ q \end{bmatrix}$$

The strict conditions for stability of $A^V_{occ}$, assuming $K_2 > 0$ and $w > 0$, are $K_2(w-\alpha) < w$ and $K_2(w-2\alpha) + 2(2-w) > 0$. If $K_2$ is chosen such that these stability conditions are met, the density state will converge to:

$$\rho^V_{ss} = \begin{bmatrix} \rho^V_{1ss} \\ \rho^V_{2ss} \\ \rho^V_{3ss} \end{bmatrix} = \begin{bmatrix} \rho_j - \frac{1-\alpha}{w} q - \frac{\alpha}{w} f_d \\ \frac{1}{K_2}(K_1 - f_d + q) \\ \frac{1}{v} q \end{bmatrix} \tag{6}$$

It can be seen that $\rho^V_{1ss} > \rho_c$ for all values of $\alpha$, $w$, $\rho_j$, $\rho_c$ and $f_d$ conforming to (1). Therefore, the only possible transitions out of `UC-V` are to `UC-IV` or `CC-V`. Otherwise the system will remain in `UC-V`. Notice that a transition directly to `CC-VI` is not possible, since it requires, at the instant of the transition, that $w(\rho_j - \rho_2) = v\rho_c > v\rho_3$, which is characteristic of `CC-V`.

Whether the eventual transition is to `UC-IV` or to `CC-V` will depend on the value of $\rho_{2ss}$. If $\rho_{2ss} > \rho_c$, the system will go to `CC-V`. If $\rho_{2ss} < \rho_c$ and also $v\rho_{2ss} < w(\rho_j - \rho_{1ss}) - \alpha r_{ss}$, the `UC-IV` transition will occur. Otherwise, the system will remain in `UC-V`. These conditions are easily translated into conditions on the controller and the model parameters utilizing Eq. (6).

A similar reasoning can be applied to the remaining modes of the system. Table 5 collects the steady state values for each of the six dynamic modes. For *feedback* modes `V` and `VI`, the result assumes that $K_2$ has been selected to stabilize the stabilizable states of the system. The ranges of $K_2$ that achieve this are given in Table 6. With some manipulation, the conditions of Table 6 can be reduce to $K_2 \in [0, \bar{K}_2]$ with

$$\bar{K}_2 = \begin{cases} \frac{(w-2)^2}{2\alpha - w} & \text{if } w < \alpha \\ \texttt{min}[\frac{(w-2)^2}{2\alpha - w}, \frac{w}{w-2}] & \text{if } \alpha < w < 2\alpha \\ \frac{w}{w-2} & \text{if } w > 2\alpha \end{cases}$$

A complete list of the possible transitions with %-Occ is given below.

**Table 5:** Steady-state behavior with %-Occ

| | |
|---|---|
| `I` | $\begin{bmatrix} \frac{1}{v}[(1-\frac{1}{v}K_2)q + K_1] & \frac{1}{v}q & \frac{1}{v}q \end{bmatrix}^T$ |
| `II` | $\begin{bmatrix} \infty & -\infty & \frac{1}{v}q \end{bmatrix}^T$ |
| `III` | $\begin{bmatrix} \frac{1}{v}[K_1 - K_2(\rho_j - \frac{1}{w}f_d) + f_d] & \rho_j - \frac{1}{w}f_d & -\infty \end{bmatrix}^T$ |
| `IV` | $\begin{bmatrix} -\infty & \frac{1}{v}q & \frac{1}{v}q \end{bmatrix}^T$ |
| `V` | $\begin{bmatrix} \rho_j - \frac{1-\alpha}{w}q - \frac{\alpha}{w}f_d & \frac{1}{K_2}(K_1 - f_d + q) & \frac{1}{v}q \end{bmatrix}^T$ |
| `VI` | $\begin{bmatrix} \frac{1}{K_2+w}[(w\rho_j - f_d)(1+\frac{\alpha}{w}K_2) + (1-\alpha)K_1] \\ \frac{1}{K_2+w}[K_1 + w\rho_j - f_d] \\ -\infty \end{bmatrix}$ |

**Table 6:** Stable gains for %-Occ

| | |
|---|---|
| `V` | $K_2(w-\alpha) < w \;;\; K_2 > 0$<br>$K_2(w-2\alpha) > 2(w-2)$ |
| `VI` | $w(w-2) + K_2(w-\alpha) < 0$<br>$(w-2)^2 + K_2(w-2\alpha) > 0$ |

`CC-VI`:

$\rightarrow$ `CC-V` or `CU-III` if $\begin{cases} \alpha \in [0, \frac{\rho_c}{\rho_j - f_d/w}] \\ \alpha[(\rho_j - f_d/w)K_2 - K_1] \\ \quad + K_1 - \rho_c K_2 < f_d - v\rho_c \end{cases}$

$\rightarrow$ `CC-V` otherwise

`CC-V`:

$\rightarrow$ `UC-V` if $K_1 - \rho_c K_2 < f_d - q$

$\rightarrow$ `CC-V` if $\begin{cases} K_1 - \rho_c K_2 > f_d - q \\ K_1 - (\rho_j - \frac{1}{w}q)K_2 < f_d - q \end{cases}$

$\rightarrow$ `CC-VI` otherwise

`UC-V`:

$\rightarrow$ `CC-V` if $K_1 - \rho_c K_2 > f_d - q$

$\rightarrow$ `UC-V` if $\begin{cases} K_1 - \rho_c K_2 < f_d - q \\ K_1 - \frac{1}{v}qK_2 > f_d - q \end{cases}$

$\rightarrow$ `UC-IV` if $K_1 - \frac{1}{v}qK_2 < f_d - q$

`UC-IV`:

$\rightarrow$ `UC-V` if $K_1 - \frac{1}{v}qK_2 > f_d - q$

$\rightarrow$ `UU-I` if $K_1 - \frac{1}{v}qK_2 < f_d - q$

`CU-III`:

$\rightarrow$ `CU-II` if $\begin{cases} q < f_d \\ K_1 - (\rho_j - \frac{1}{w}f_d)K_2 < v\rho_c - f_d \end{cases}$

CU-II:

$\rightarrow$ UU-I  if $\begin{cases} q < f_d \\ K_2 > 0 \end{cases}$

UU-I:

$\rightarrow$ UU-I  if $K_1 - \frac{1}{v} q K_2 < v\rho_c - q$

Close inspection of the possible paths for the %-Occ controller reveals that only two sensible strategies exist: a high gain strategy (A), and a low gain strategy (B). The state transition diagrams resulting from these two options are illustrated in Fig. 4 and 5. They are achieved by enforcing the constraints enabling transitions CC-VI→CU-III, CU-III→CU-II, CU-II→UU-I, in addition to the following:

Strategy A (High gain): $K_1 - \frac{1}{v} q K_2 < f_d - q$
Strategy B (Low gain): $K_1 - (\rho_j - \frac{1}{w} q) K_2 > f_d - q$

Fig. 6 shows feasible regions in the $K_2/K_1$ plane. Both of these options have serious drawbacks. From the diagrams it is clear that only strategy A ensures an eventual arrival to the UU-I mode. However its additional constraint excludes the *optimal* values of $K_1$ and $K_2$. That is, those values satisfying $K_1 - \frac{1}{v} q K_2 = v\rho_c - q$ that achieve maximum throughput $f_1 = v\rho_c$. In fact, the maximum achievable flow in UU-I with the high gain strategy is $f_1 = f_d$, which is the presumed worst-case scenario if no control were applied. Therefore, strategy A does not accomplish the second control objective. On the other hand, strategy B, while possibly achieving maximum flow, cannot guarantee convergence to UU-I.

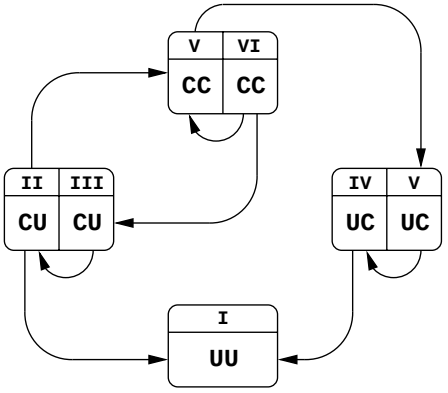


**Figure 4:** %-Occ : Strategy A

### 3.2 Alinea control

The Alinea control law was first introduced by Papageorgiou in [6]. It has since been tested in several European cities [7], where it has performed favorably as compared to %-Occ (or a variant of %-Occ since a downstream measurement was used). It is interpreted as integral feedback control of the downstream occupancy. Again relating occupancy to density, the control law for Alinea becomes:

$$r_{[k]} = r_{[k-1]} + K_r(\hat{\rho}_1 - \rho_{1[k]}) \qquad (7)$$

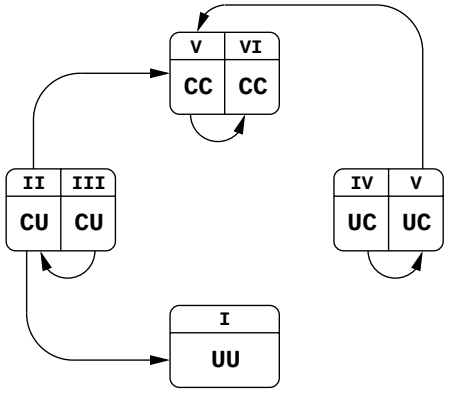


**Figure 5:** %-Occ : Strategy B

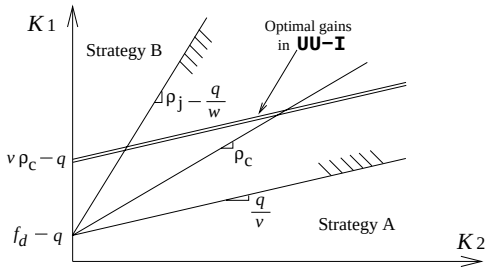


**Figure 6:** %-Occ parameter constraints

$\hat{\rho}_1$ is a target density, and $K_r$ is the feedback gain. We apply the same analytical procedure to Alinea as to %-Occ. It has been assumed in every case that $K_r > 0$, $\hat{\rho}_1 < \rho_c$, and $q < f_d$. The additional requirements on the controller gain that stabilize the stabilizable states in each of the dynamic modes are given in Table 7. With $w < v$ and $\alpha \in [0, 1]$, these are all covered by selecting $K_r \in [0, 2(2 - v)]$.

**Table 7:** Stable ranges of $K_r$

| | |
|---|---|
| I | $K_r \in [0, 2(2-v)]$ |
| II | $K_r \in [0, 2(2-v)]$ |
| III | $K_r \in [0, 2(2-v)]$ |
| IV | $K_r \in [0, 4]$ |
| V | $K_r \in [0, 2\frac{2-w}{1-\alpha}]$ |
| VI | $K_r \in [0, 2\frac{2-w}{1-\alpha}]$ |

Steady-state values of $\rho$ appear in Table 8 with $\rho_{2ss}^{VI} = \hat{\rho}_1 + \frac{\alpha}{1-\alpha}(\frac{1}{w} f_d - (\rho_j - \hat{\rho}_1)) < \hat{\rho}_1 < \rho_c$.

It is worth noting that Alinea successfully stabilizes $\rho_1$ about $\hat{\rho}_1$ in all dynamic modes where $\rho_1$ is controllable, with the exception of mode IV. The $\odot$ symbol in Table 8 is meant to indicate that, in dynamic mode IV, $\tilde{\rho}_1 = \hat{\rho}_1 - \rho_1$ behaves like an undamped oscillator (for $K_r \in [0, 4]$). Specifically, we have:

$$\tilde{\rho}_{1[k+2]} + (K_r - 2)\tilde{\rho}_{1[k+1]} + \tilde{\rho}_{1[k]} = 0 \qquad (8)$$

Analogously to with %-Occ, we list the possible transitions with Alinea. These are derived with the prior assumption that $K_r \in [0, 2(2 - v)]$.

**Table 8:** Steady-state behavior with Alinea

| | |
|---|---|
| I | $\left[\hat{\rho}_1 \quad \frac{1}{v}q \quad \frac{1}{v}q\right]^T$ |
| II | $\left[\hat{\rho}_1 \quad -\infty \quad \frac{1}{v}q\right]^T$ |
| III | $\left[\hat{\rho}_1 \quad \rho_j - \frac{1}{w}f_d \quad -\infty\right]^T$ |
| IV | $\left[\odot \quad \frac{1}{v}q \quad \frac{1}{v}q\right]^T$ |
| V | $\alpha \neq 1$: $\left[\hat{\rho}_1 \quad -\infty \quad \frac{1}{v}q\right]^T$<br>$\alpha = 1$: $\left[\rho_j - \frac{1}{w}f_d \quad -\infty \quad \frac{1}{v}q\right]^T$ |
| VI | $\alpha \neq 1$: $\left[\hat{\rho}_1 \quad \rho_{2ss}^{VI} \quad -\infty\right]^T$<br>$\alpha = 1$: $\left[\rho_j - \frac{1}{w}f_d \quad -\infty \quad -\infty\right]^T$ |

| | | | |
|---|---|---|---|
| CC-VI: | → CC-V or CU-III | if | $\alpha \neq 1$ |
| | → CC-V | if | $\alpha = 1$ |
| CC-V: | → UC-V or CU-II | if | $\alpha \neq 1$ |
| | → UC-V | if | $\alpha = 1$ |
| UC-V: | → UC-IV | always | |
| UC-IV: | → UC-V or UU-I | always | |
| CU-III: | → CU-II | always | |
| CU-II: | → UU-I | always | |
| UU-I: | → UU-I | always | |

State transition diagrams for the two cases, $\alpha \neq 1$ and $\alpha = 1$, are shown in Fig. 7 and 8. Both cases contain loops, which at first glance appear to make it possible for the system to get caught in the UC congestion mode. It can be shown however, based on Eq. (8), that the transition UC-V→UC-IV must necessarily be followed by UC-IV→UU-I (as $\rho_1$ is decreasing when it enters UC-IV, it must continue to decrease until UU-I is reached). Having broken this loop, it is apparent that, for any value of $\alpha \in [0, 1]$, the system will eventually reach the UU-I mode, and that once there, $\rho_1$ will approach $\hat{\rho}_1$.

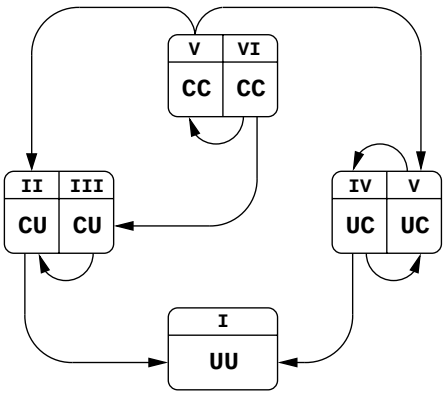


**Figure 7:** Alinea with $\alpha \in [0, 1)$

## 4 Conclusions

One of the desired model specifications outlined in the Introduction, was that it should include the observed difference in maximum flows between the uncongested and congested regimes ($v\rho_c > f_d$). This turned out to be an important requirement, as it was found in the analysis that a high gain %-Occ strategy could a most

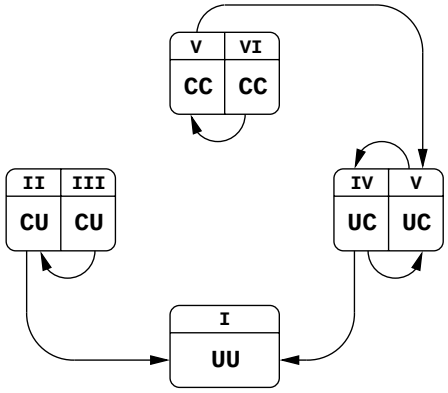


**Figure 8:** Alinea with $\alpha = 1$

provide a steady state throughput of $f_d$. The low gain strategy, on the other hand, resulted in higher flows in the UU-I mode, but was not always able to eliminate congestion. In regards to Alinea, it was found that the range of controller parameters $K_r \in [0, 2(2-v)]$ and $\rho_j - \frac{1}{w}f_d < \hat{\rho}_1 < \rho_c$ satisfied the control objectives. These results seem to suggest that Alinea is a superior approach to %-Occ, however no conclusions were reached with respect to their relative performances here. In particular, we did not investigate how quickly Alinea or high-gain %-Occ recover from congestion. This is an important consideration since it is closely related to travel time. Another important question is how Alinea performs when only upstream measurements are available, and how controller parameters should be selected in this situation. These issues, along with improved controller designs using this model, are left as future work.

## References


[1] J. Banks. Two-capacity phenomenon at freeway bottlenecks: A basis for ramp metering? *Transportation Research Record*, 1320, 1991.

[2] F. Hall and K. Agyemang-Duah. Freeway capacity drop and the definition of capacity. *Transportation Research Record*, 1320, 1991.

[3] M. Papageorgiou and A.los Kotsialos. Freeway ramp metering: An overview. In *IEEE Intelligent Transportation Systems*, October 2000.

[4] C. Daganzo. The Cell Transmission Model: A Dynamic Representation of Highway Traffic Consistent with the Hydrodynamic Theory. *Transportation Research - B*, 28(4), 1994.

[5] C. Daganzo. The Cell Transmission Model, Part II: Network Traffic. *Transportation Research - B*, 29(2), 1995.

[6] M. Papageorgiou, H. Hadj-Salem, and J. Blosseville. Alinea: A local feedback control law for on-ramp metering. *Transportation Research Record*, 1320, 1991.

[7] M. Papageorgiou, H. Hadj-Salem, and F. Middelham. Alinea local ramp metering: Summary of field results. *Transportation Research Record*, 1603, 1998.